Measurement 225 (2024) 114030

Contents lists available at ScienceDirect

Measurement

journal homepage: www.elsevier.com/locate/measurement

High sensitivity detection of ethanol solution based on waveguide resonant cavity combined with metamaterials

Yao Zhang [a], Leijun Xu [a,*], Jianfeng Chen [a], Xue Bai [a], Xiao Zhou [a]

[a] School of Electrical and Information Engineering, Jiangsu University, Zhenjiang 212013, China

ARTICLE INFO

Keywords:
Ethanol solution
Waveguide resonant cavity
Metamaterial
Multilayer medium theory
Sensitivity

ABSTRACT

In this article, a novel methods of ethanol solution detection based on the waveguide resonant cavity and metamaterial, is proposed. Different from the traditional detection methods, our proposed technique has the advantages of alleviating the negative effects of the volatility and high loss of ethanol, and result in the improvement of sensitivity. By opening a gap on the narrow side of the resonant cavity properly, the measured object, i.e., the ethanol solution, can flow into the cavity, without the adopting of additional tube as the fluid channel. Moreover, since the constant volume and metallic shield of the cavity, the test setup can keep stable, which is advisable for the accurate detection under complex environment. In order to enhance the interaction between electromagnetic waves (EMWs) and ethanol solution, the metamaterial structure of the split-ring resonant (SRR) is employed and integrated with the resonant cavity. Multilayer medium theory is developed to analyze the propagation of the EMWs and optimize the performance. The proposed method can detect the variation of ethanol concentration from 0 % to 100 %, by changing the resonant frequency from 1.56 GHz to 2.44 GHz (0.88 GHz shift), exhibiting a sensitivity of 0.8 % and a maximum error of only 1.4 %. The simulation and test results are consistent, demonstrating the feasibility of using the waveguide resonant cavity and metamaterial for highly sensitive and accurate detection of ethanol.

1. Introduction

Ethanol, as a solvent [1,2], is widely used in fields such as medicine, food industry, and agricultural production [3–5]. However, its volatility and flammability make it difficult to accurately monitor its concentration during practical applications [6–8], especially in the safety production fields of beverages, drugs, and fuels, where ethanol concentration is a key indicator in the manufacturing process [9,10]. By detecting ethanol concentration, product quality can be ensured and problems caused by insufficient or excessive ethanol concentration can be avoided [11,12]. In addition, with economic development, issues such as drunk driving, alcohol abuse, and alcohol poisoning have become increasingly prominent in the global public safety and health field [13–15]. Therefore, precise detection of ethanol concentration is crucial for ensuring public health and safety.

In the past few decades, there have been many traditional methods for detecting ethanol, including distillation [16,17], spectrophotometry [18], gas chromatography [19,20], gas-mass spectrometry [21,22], spectral analysis [23], and so on [24–26]. However, the traditional distillation and spectrophotometry methods are known for their low accuracy and large errors [27]. On the other hand, gas chromatography, gas-mass spectrometry, and spectral analysis methods are often expensive and require highly skilled operators, making them unsuitable for routine production application [28]. Therefore, there is an urgent need to develop new techniques for the accurate, highly sensitive, and cost-effective detection of ethanol concentration in routine testing.

In recent years, metamaterials have emerged as an attractive material with unique properties that are not found in natural materials [29,30]. These properties include negative refractive index and the electromagnetically induced transparency effect [31]. By designing various structures of SRR, metamaterial sensors have become highly sensitive to changes in the dielectric constant caused by the addition of liquid samples, making them popular among sensor researchers. Some progress has been made in the detection of mixed solutions [32–39]. For instance, literature [40] successfully measured the concentration of ethanol in water by inserting a glass capillary tube inside the substrate of a Complementary split-ring resonant (CSRR) structure. Similarly, literature [41] developed a microwave sensor with a CSRR to detect different

* Corresponding author.
E-mail addresses: 2112107016@stmail.ujs.edu.cn (Y. Zhang), xlking@ujs.edu.cn (L. Xu), chenjianfengnjnu@163.com (J. Chen), baixue@ujs.edu.cn (X. Bai), zxzhouxiao1998@163.com (X. Zhou).

https://doi.org/10.1016/j.measurement.2023.114030
Received 27 October 2023; Received in revised form 7 December 2023; Accepted 11 December 2023
Available online 13 December 2023

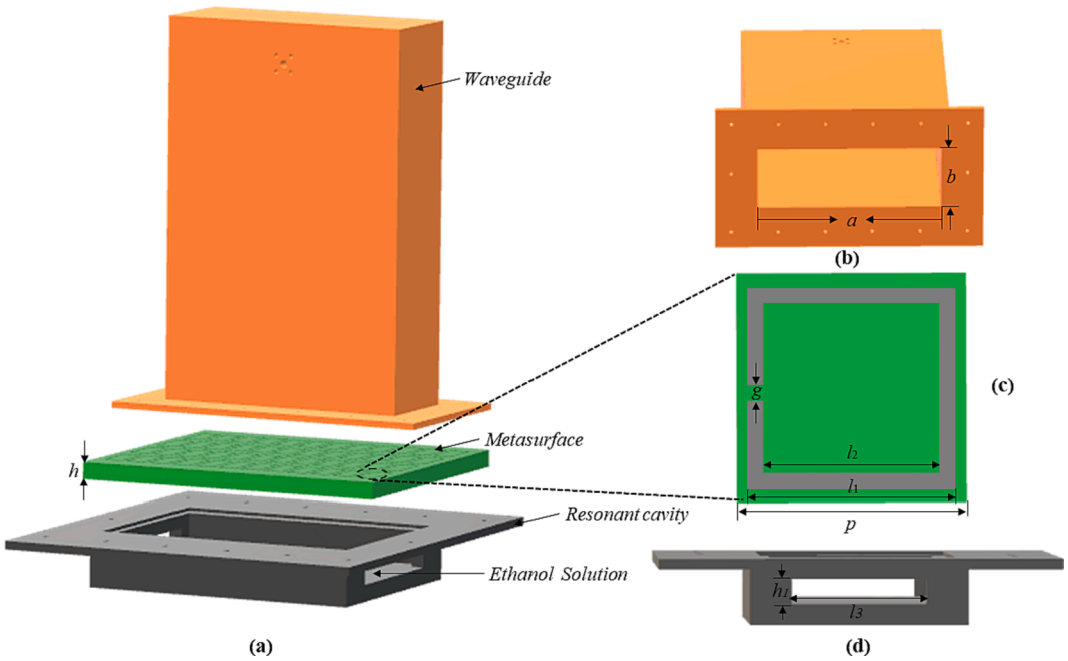

Fig. 1. The structure diagram of the sensor: (a) Three-dimensional view. (b) Elevation view of the waveguide. (c) Top view of the metamaterial. (d) Side view of the resonant cavity.

concentrations of ethanol solution by placing the sample in a pipette in the middle of the sensor. The sensor has a resonant frequency shift of only 0.2 GHz as the ethanol concentration changes from 0 % to 100 %. Reference [42] designed a novel metamaterial sensor, consisting of a large split-ring resonator (SRR) and three small SRRs positioned on the front and back sides. This sensor is used for the detection of milk and dairy products by placing liquid samples on a sample holder, and it was observed that the maximum resonance frequency shift is only 0.14 GHz. However, most of the above-mentioned microwave sensors for fluid channel detection are composed of a liquid carrier tube, which not only limits the volume of liquid but also affects the sensitivity of the sensor. Therefore, it becomes challenging to distinguish small changes in the dielectric constant and achieve high sensitivity detection. In order to overcome these challenges, literature [43] implemented a double split-ring resonant (DSRR)-based microwave sensor at 2.45 GHz, which detected ethanol solution with concentrations of 20 %-80 %. While the sensor has a resonant frequency shift of 0.85 GHz, exposing the ethanol solution to air during the experiment made it prone to volatilization, leading to significant measurement errors and inaccurate results. As a result, achieving high sensitivity and precise detection of liquid solutions in the microwave frequency band remains challenging.

This study presents a high-sensitivity microwave fluidic sensor based on waveguide resonant cavity and metamaterials. This sensor can detect ethanol–water solutions with concentrations ranging from 0 % to 100 %. We designed a metamaterial sensor based on the SRR structure and placed the ethanol solution with different concentrations directly beneath the metamaterial sensor. By creating a gap on the narrow side of the resonant cavity, the ethanol solution can flow into the cavity quickly. To improve the interaction between electromagnetic waves and the measured solution, a metamaterial sensor based on the SRR structure is coupled through the resonant cavity. Furthermore, since the ethanol solution inside the resonant cavity is not volatile, the detection of 0 %–100 % ethanol solution can achieve high sensitivity and accuracy. Compared to the conventional detection method of placing the measured solution above the metamaterial sensor, the proposed method demonstrates a significantly larger resonant frequency shift when detecting ethanol solution. When the ethanol concentration changes from 0 % to 100 %, the sensor exhibits a resonant frequency shift of 0.88 GHz. This study provides a new practical approach for detecting mixed solutions.

2. Materials and experimental equipment

2.1. Sample and materials

The ethanol (≥99.7 %) was purchased from Jiangsu Qiangsheng Functional Chemical Co. Ltd. Distilled water was purchased from Mellon Supermarket of Jiangsu University and was not further purified. The required amount of ethanol solution was mixed with distilled water to prepare ethanol concentrations of 0 %, 20 %, 40 %, 60 %, 80 %, and 100 %. Each concentration was prepared five times for repeatability.

The reflection curve of ethanol solution at different concentrations was collected by connecting the SMA interface of the waveguide to the signal output port of a vector network analyzer (AV3656B, CLP 41, Anhui, China). 30 sets of parameters were obtained for each ethanol solution concentration by repeating the sampling five times. Finally, the parameters from five sets of ethanol solution with the same concentration were averaged to obtain the reflection curve for ethanol solution ranging from 0 % to 100 %. All measurements were conducted at a temperature of 25 ± 1 °C.

2.2. Microwave sensor design

The schematic diagram of the proposed sensor is shown in Fig. 1(a), which consists of a rectangular waveguide and a resonant cavity. The resonant cavity comprises a metamaterial and a cavity. The rectangular waveguide cell section is shown in Fig. 1(b), with a wide edge size of a = 120 mm and a narrow edge size of b = 40 mm. The designed waveguide can be used in the range of 1.25 GHz–3.75 GHz and achieves a return loss of less than −10 dB in the range of 1.59 GHz-2.8 GHz, with an absolute bandwidth of 1.21 GHz and a relative bandwidth of 70.15 %. The metamaterial cell covering the resonant cavity is designed according to the transmission band of the waveguide, with an array cell of 12 * 4. Side and top views of the cell layout of the SRR are shown in Fig. 1(a) and 1(c). The metamaterial consists of two layers: a dielectric substrate (Fr4) and a metal layer (Cu). The detailed structural parameters are as

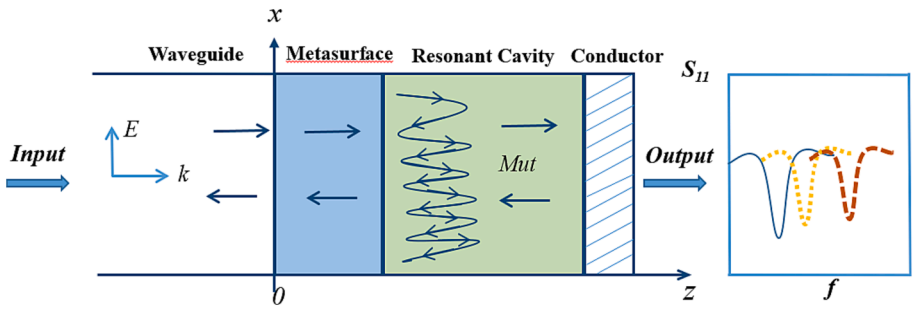

Fig. 2. Overall working principle of the sensor.

follows: $p = 10$ mm, $l_1 = 7.8$ mm, $l_2 = 7.2$ mm, g = 0.4 mm, and the thicknesses of the dielectric substrate and metal layer are $h = 1$ mm and $t = 0.035$ mm, respectively. In the simulations, the dielectric constant of the substrate layer is set to $\varepsilon_r = 4.3$, the loss angle tangent is set to tan $\delta = 0.02$, and the conductivity of Cu is set to 5.8×10^7 S/m. Additionally, the cavity part located below the metamaterial as shown in Fig. 1(d) is used as a fluid channel to load the ethanol solution. Gaps are opened on both sides of the narrow side of the cavity symmetrically with a width of $l_2 = 32$ mm and a height of $h_1 = 3$ mm, making the ethanol solution flow smoothly into the cavity and facilitating the measurement of the solution.

3. Design details

3.1. The overall working principle

An incident electromagnetic wave propagates perpendicularly through the coaxial port into the air waveguide. Upon reaching the metasurface, a portion of the electromagnetic energy is reflected, forming a reflected wave, while another portion continues to propagate through the metasurface as a transmitted wave. The transmitted wave couples with the metasurface, generating strong electromagnetic resonance. Within the resonant cavity, partially transmitted electromagnetic energy encounters the ethanol solution, leading to reflection and transmission similar to that of the metasurface. As the cavity's bottom is a metal conductor, a portion of the electromagnetic energy only reflects off the surface, forming reflection waves. The ethanol solution, located below the metasurface in the cavity, exhibits a standing wave phenomenon. Changes in ethanol concentration cause corresponding changes in the dielectric environment of the metasurface structure, resulting in a shift of the resonant frequency. Sensing tests are conducted by analyzing the frequency shift of the resonant peak. The overall working principle is illustrated in Fig. 2. According to the theory of vertical incidence of uniform plane waves on the partitioned interface of multilayer media [44,45], we simplify the analysis by equating it to a terminal short-circuit layered waveguide model. We derive reflection coefficients and resonant frequencies of ethanol solution at different concentrations. Assuming that the incident wave is an electric field along the x-direction, the electric and magnetic fields of the incident wave in the air waveguide are:

$$E_{1i}(z) = e_x E_{1im} e^{-j\beta_1 z} \tag{1}$$

$$H_{1i}(z) = e_y \frac{1}{\eta_1} E_{1im} e^{-j\beta_1 z} \tag{2}$$

where E_{1im} is the incident wave electric field amplitude, η_1 is the intrinsic impedance of the air waveguide, and β_1 is the wave number of the air waveguide. Then the electric and magnetic fields of the reflected wave are:

$$E_{1r}(z) = e_x E_{1rm} e^{j\beta_1 z} = e_x \Gamma_1 E_{1im} e^{j\beta_1 z} \tag{3}$$

$$H_{1r}(z) = -e_y \frac{1}{\eta_1} E_{1rm} e^{j\beta_1 z} = -e_y \frac{1}{\eta_1} \Gamma_1 E_{1im} e^{j\beta_1 z} \tag{4}$$

Where, E_{1rm} is the electric field amplitude of the reflected wave, Γ_1 is the reflection coefficient at the interface between the air waveguide and the solution to be measured. The synthesized wave in the waveguide is:

$$E_1(z) = e_x E_{1im}\left(e^{-j\beta_1 z} + \Gamma_1 e^{j\beta_1 z}\right) \tag{5}$$

$$H_1(z) = e_y \frac{1}{\eta_1} E_{1im}\left(e^{-j\beta_1 z} - \Gamma_1 e^{j\beta_1 z}\right) \tag{6}$$

And so on, the electromagnetic waves in the solution to be measured are:

$$E_2(z) = e_x \tau_1 E_{1im}\left(e^{-j\beta_2 (z-d)} + \Gamma_2 e^{j\beta_2 (z-d)}\right) \tag{7}$$

$$H_2(z) = e_y \frac{1}{\eta_2} \tau_1 E_{1im}\left(e^{-j\beta_2 (z-d)} - \Gamma_2 e^{j\beta_2 (z-d)}\right) \tag{8}$$

Where τ_1 is the transmission coefficient at the interface between the air waveguide and solution to be measured, Γ_2 is the reflection coefficient at the interface between the solution to be measured and the metal conductor, is the intrinsic impedance of the solution to be measured, and β_2 is the wave number of the solution to be measured.

Since the lowest part is a metal conductor, the conductivity is 0, $\eta_3 = 0$, $\Gamma_2 = -1$. And the electric and magnetic fields are equal at the interface between the air waveguide and the measured solution, which can be obtained:

$$\eta_1 \frac{1 + \Gamma_1}{1 - \Gamma_1} = \eta_{ef} \tag{9}$$

Where $\eta_{ef} = \eta_2 j\tan(\beta_2 d)$. The reflection coefficient at the interface between the air waveguide and the solution to be measured is obtained as:

$$\Gamma_1 = \frac{\eta_{ef} - \eta_1}{\eta_{ef} + \eta_1} \tag{10}$$

When $\Gamma_1 = -1$ or 1 occurs in the case of standing wave, the resonant frequency f can be obtained:

$$f = \frac{c}{2\sqrt{\varepsilon_r}} \sqrt{\left(\frac{2}{\lambda}\right)^2 + \left(\frac{1}{a}\right)^2} \tag{11}$$

Where c is the speed of light, a is the length of the wide side of the waveguide, $\lambda = 4*d/(2n + 1)$ is the wavelength, n is 1, 3, 5……., ε_r is the dielectric parameter of the measured solution.

3.2. Metamaterial design and resonance performance analysis

Since the performance of the sensor is large influenced by its structural parameters, we utilized the control variable method to optimize the structural parameters of the metamaterial. Specifically, we kept the remaining parameters constant and varied the opening size g of the SRR

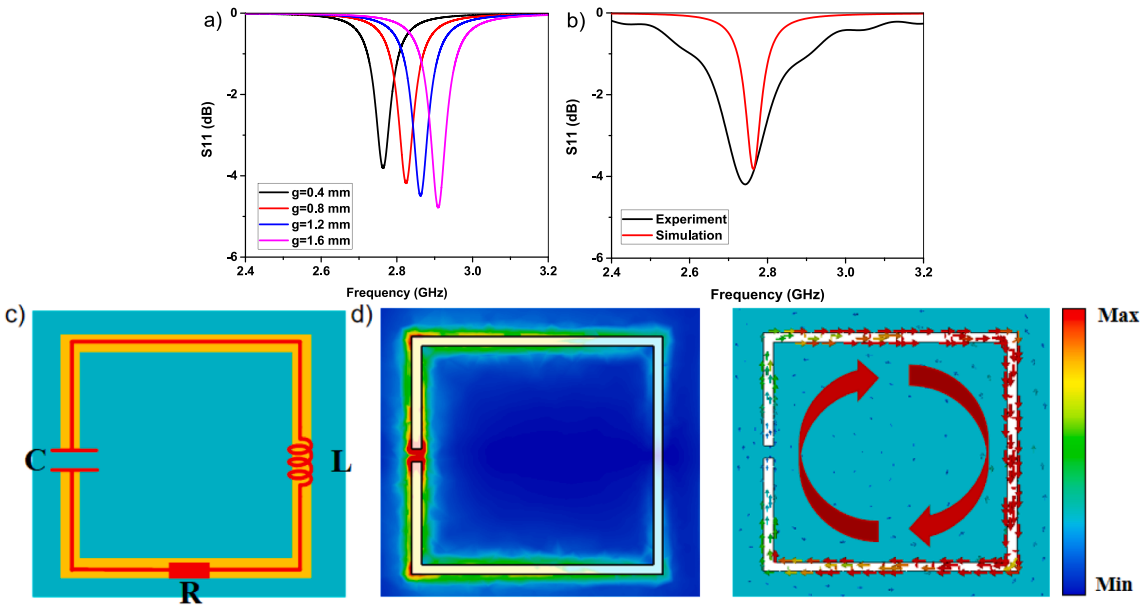

Fig. 3. (a) Influence of structural parameter *g* on reflection spectrum. (b) The reflection curves obtained by simulation (red line) and experiment (black line). (c) The equivalent circuit model of the sensor. (d) Corresponding electric field and surface current distribution at the resonant frequency of 2.76 GHz.

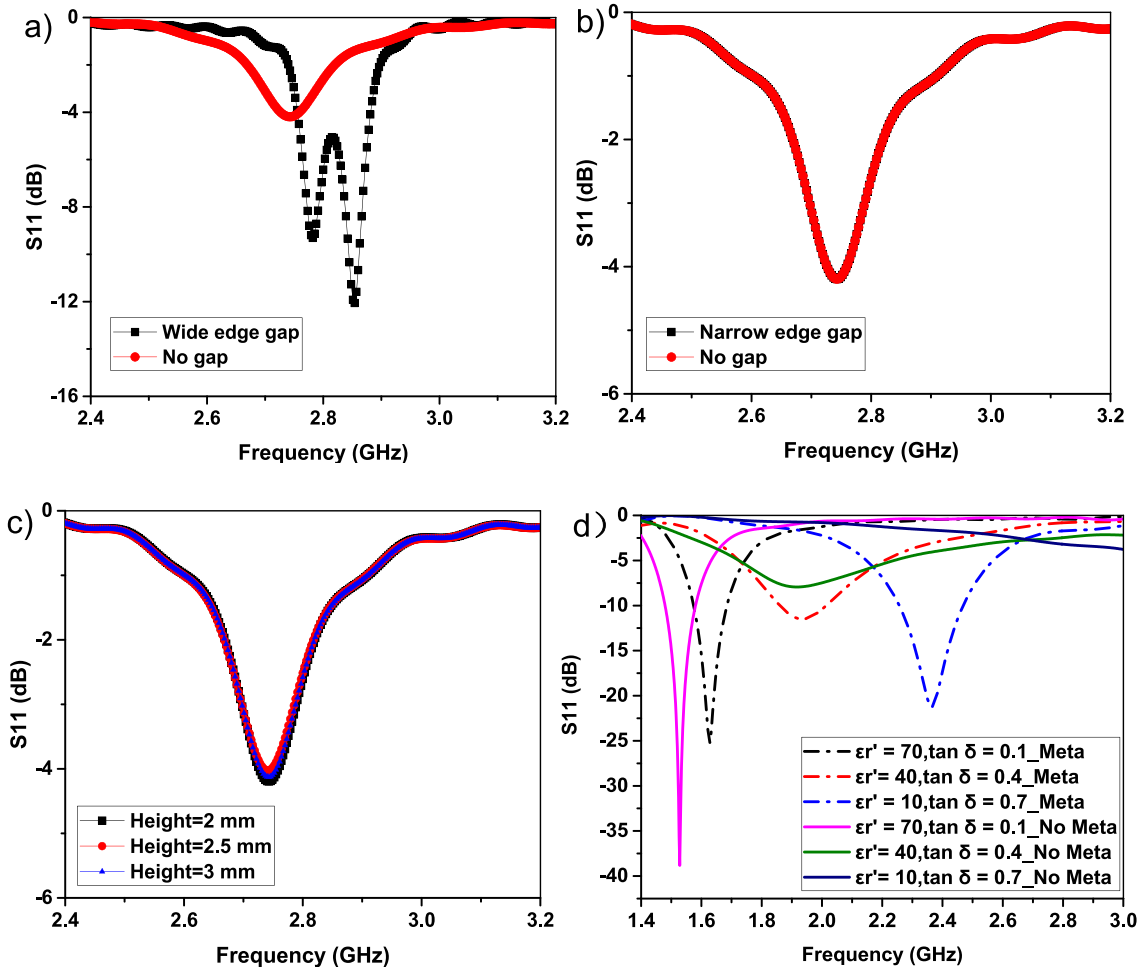

Fig. 4. (a) Comparison of reflection curves of wide-edge cavity with a gap and without gap. (b) Comparison of reflection curves of narrow cavity with the gap and without gap. (c) Relation between reflectance and frequency as resonant cavity height varies from 2 mm to 3 mm. (d) Comparison of reflection curves between placing metamaterials in the cavity and not placing metamaterials.

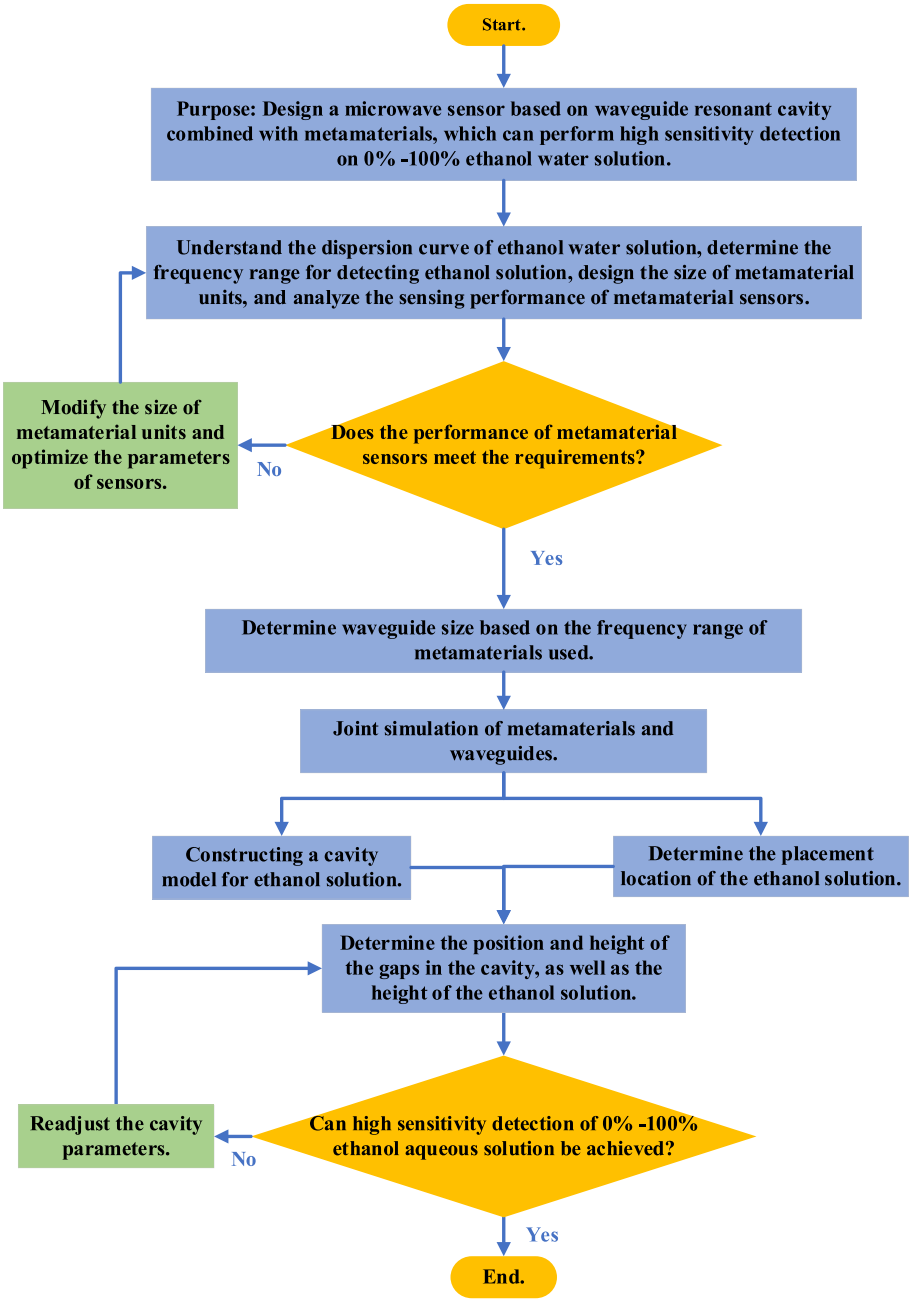

Fig. 5. Flowchart of the proposed sensor design.

from 0.4 mm to 1.6 mm, with intervals of 0.4 mm. The resulting reflection spectrum is presented in Fig. 3(a), revealing that an opening size of 0.4 mm produces the sharpest resonance peak and the largest Q value. Since the metamaterial will be used for measuring ethanol concentrations ranging from 0 % to 100 %, a larger Q value is required. Therefore, we set the opening size of the metamaterial SRR structure to 0.4 mm for both subsequent simulations and experimental designs.

To verify the accuracy of the simulation, we compared the reflection curves of the Split Ring Resonator (SRR) that were simulated and tested, as shown in Fig. 3(b). The simulation results are in red, while the black lines represent the test results. Upon comparison, we observed that the experimental results closely matched the simulation results, with the deviation being primarily caused by processing errors. It is also possible that the actual FR4 loss is higher than the loss used in the simulation, resulting in a slightly lower magnitude for the experimental test. Moreover, since the experimental processing period is finite and the actual simulation period is infinite, the difference in the model may also lead to differences in the reflection curve. The sensor resonates at a frequency of 2.76 GHz. To better understand the fundamental principle of resonance generation in the SRR structure, we examined the electric field and surface current at this resonant frequency, as shown in Fig. 3 (d). The left figure shows that the electric field is mainly concentrated at the gap, and this resonance can be regarded as the LC resonance mode. On the other hand, the right figure shows that the surface current on the SRR forms a circle, creating a magnetic dipole in the incident direction. According to the principle of equivalent circuit, the coupling between the opening gap g of SRR and the structural unit is regarded as the equivalent capacitance C, the effect of the metal wire part through which the induced current flows is regarded as the equivalent inductance L, and the ohmic loss generated by the induced current flow is equivalent to the resistance R, as shown in Fig. 3(c).

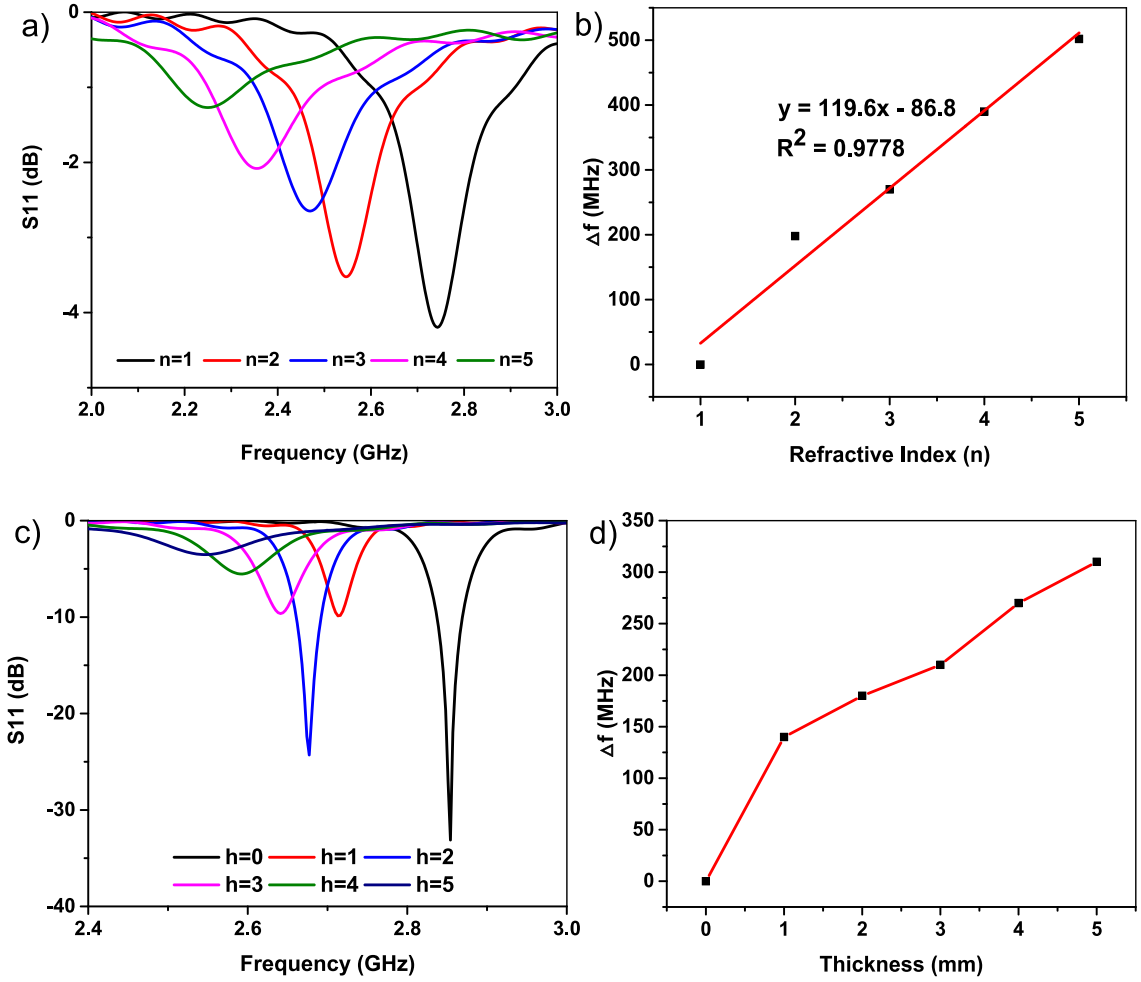

Fig. 6. (a) Relation between reflectance and frequency for the analyte thickness of 5 mm and refractive index from 1 to 5. (b) The frequency shift △f as a function of refractive index of analyte extracted from (a). (c) Relation between reflectance and frequency for the refractive index of 2 and analyte thickness ranges from 0 to 5 mm. (d) The frequency shift △f as a function of analyte thickness as extracted from (c).

Table 1
Reference value of complex dielectric constant of water–ethanol mixture.

Water	Ethanol	ε	ε
100 %	0 %	78.30	6.71
80 %	20 %	67.47	10.40
60 %	40 %	54.97	15.53
40 %	60 %	38.95	16.12
20 %	80 %	21.21	14.11
0 %	100 %	6.89	6.56

3.3. Metamaterial and resonant cavity design details

The resonant cavity we designed is located directly below the waveguide to house the metamaterial and the liquid being measured. To allow for the smooth flow of liquid, we need to create gaps at both the wide and narrow sides of the cavity. Firstly, we created a gap on the wide side of the cavity and compared the results with those obtained without the gap, as shown in Fig. 4(a). We found that compared to the no-gap scenario, opening a gap on the wide side resulted in two resonance points due to the interruption of the surface current. This suggests that the wide edge of the cavity can affect the reflection result. To prevent the surface current from being cut off, we created a gap on the narrow side of the cavity, and the results are shown in Fig. 4(b). The results of creating a gap on the narrow side were similar to those obtained without any gaps, indicating that we can create a gap on the narrow side to facilitate the flow of the liquid being measured into the cavity. This enables accurate and rapid detection of the measured solution. To investigate whether the gap height affects the reflection results, we varied the gap height between 2 mm and 3 mm with an interval of 0.5 mm. The resulting reflection curves are shown in Fig. 4(c), where we obtained reflection curves for gap heights of 2 mm, 2.5 mm and 3 mm. The results showed that the gap height did not have any significant effect on the reflection curve. In order to ensure rapid inflow of the measured liquid, we set the gap height of the cavity to 3 mm. To better illustrate the design process of the proposed microwave sensor, the flowchart is depicted in Fig. 5 [46].

To demonstrate that metamaterials can enhance the interaction between electromagnetic waves and the target material, we conducted simulation comparisons under two scenarios: one with metamaterial placed inside the cavity and the other without metamaterial. The reflection curves and resonant frequency inside the cavity without metamaterial was obtained using Formula (10) and Formula (11). We assumed a constant thickness of 5 mm for the target material, with different relative permittivity (ε_r') set to 70, 40 and 10, along with corresponding loss tangents (tan δ) of 0.1, 0.4 and 0.7. Through simulation, we obtained reflection curves for target materials with different dielectric parameters, as shown in Fig. 4(d). When metamaterial was placed inside the cavity, as the dielectric constant (ε_r') of the target material varied from 70 to 10, and the corresponding loss tangent (tan δ) increased from 0.1 to 0.7, the resonant points could clearly distinguish different dielectric parameters of the target material. However, when

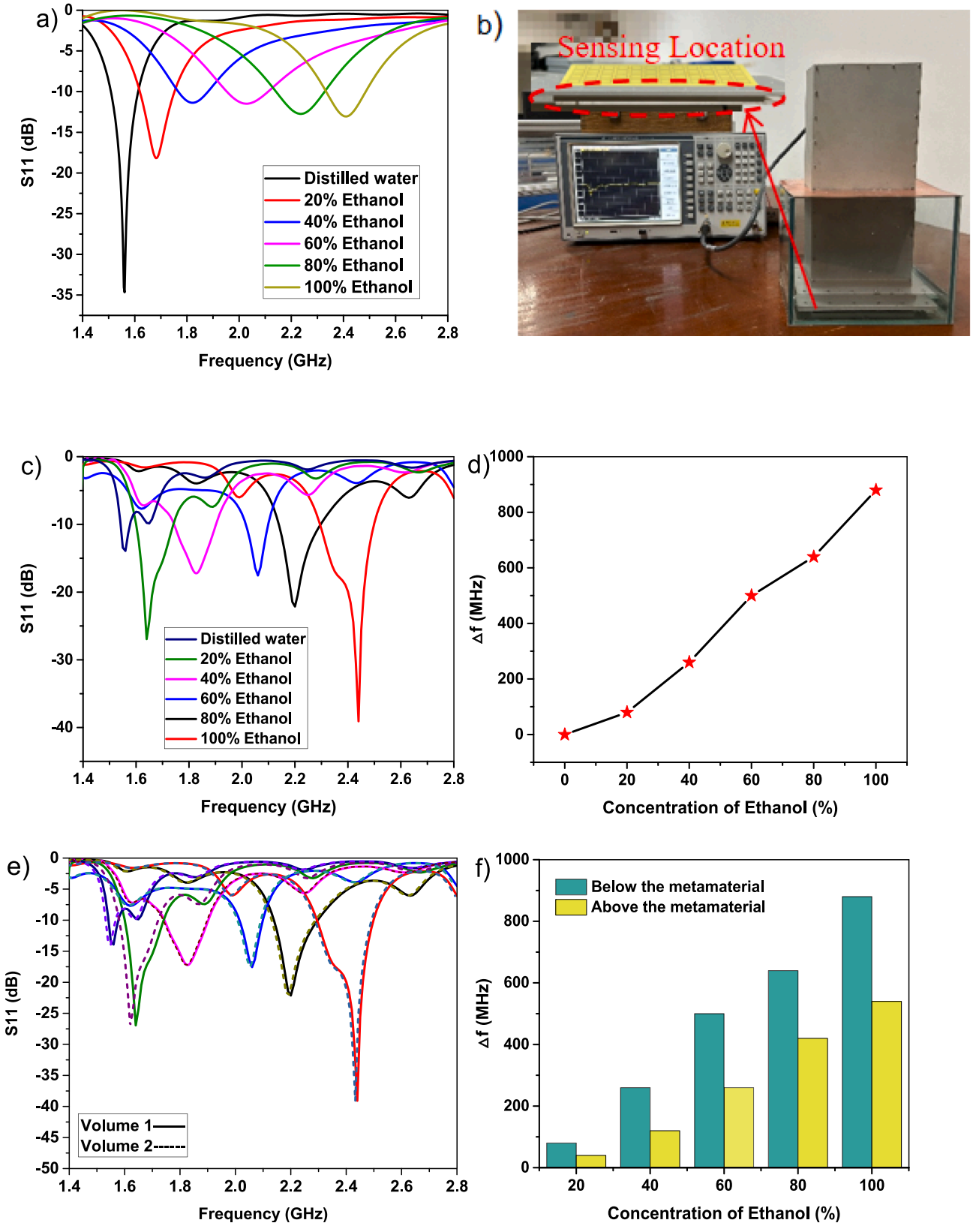

Fig. 7. (a) The variation of reflectance with frequency obtained from the simulation is influenced by different ethanol concentrations. (b) Measurement of different ethanol concentrations using the VNA network analyzer. (c) The variation of the tested reflectance with frequency is influenced by different ethanol concentrations. (d) The relationship between the change in resonance frequency and the concentration of ethanol. (e) The effect of two different volumes of ethanol solution on the resonance frequency. The volume 1 is 24 mL, and the volume 2 is 34 mL. (f) Comparison of the change in frequency shift with ethanol concentration when the test object is above and below the metamaterial.

Table 2
The values of error for each ethanol solution.

Volume Fraction of Ethanol	f_{SM}	f_{SS}	Error
0 %	1.56	1.56	0
20 %	1.64	1.68	1.4 %
40 %	1.82	1.82	0
60 %	2.06	2.02	1.4 %
80 %	2.20	2.24	1.4 %
100 %	2.44	2.41	1.1 %

there was no metamaterial inside the cavity, it was more challenging to distinguish between target materials with ε_r' of 40 and 10, especially when tan δ was 0.4 and 0.7. In the case of tan $\delta = 0.7$, the resonant points were no longer visible in the curve. Therefore, it is essential to place metamaterial inside the cavity to enhance the interaction between electromagnetic waves and the target material.

4. Results and discussion

4.1. Analysis of sensing performance based on metamaterial sensors

To evaluate the performance of the designed metamaterial-based sensor for sensing measurements, we investigated the impact of the refractive index and thickness of the measured object on the sensitivity of sensor. For the simulation of ethanol solution concentration detection, we placed the measured object beneath the substrate of the metamaterial sensor. We first assumed a material thickness of 5 mm, and obtained the reflection spectra of the measured materials with varying refractive indices using simulation, as shown in Fig. 6(a). We found that as the refractive index changed from 1 to 5, the resonant frequency red-shifted from 2.74 GHz to 2.24 GHz. To quantify the sensitivity of sensor, we plotted the functional relationship between the resonance frequency offset and the refractive index change in Fig. 6(b). We observed that the deviation of resonance frequency was linearly proportional to the change in refractive index Δn. In fact, the thickness of the measured object also affects the performance of sensor. Assuming a refractive index of 2 for the measured object, we obtained the results by changing the thickness h of the measured object, as shown in Fig. 6(c). As the thickness increased from 0 to 5 mm, the resonant frequency red-shifted from 2.85 GHz to 2.54 GHz. In order to better visualize the influence of the thickness of the measured object on the sensor sensitivity, we plotted the relationship between the resonant frequency shift and the thickness in Fig. 6(d). We found that when the thickness of the measured object varied from 0 to 1 mm, the maximum resonant frequency shift of the sensor was 140 MHz. This represents the frequency shift Δf with or without the object on the sensor surface. When the designed sensor was used with the measured object, it demonstrated good sensing performance. It is worth noting that the resonant frequency was not linearly red-shifted.

4.2. Quantitative analysis of ethanol solutions

In order to demonstrate the significant effect of the designed microwave sensor on ethanol solution detection, we first constructed a detection model using CST software. By varying the dielectric parameters of ethanol solution, Table 1 shows reference value obtained from the literature [47,48], allowing us to obtain the reflection curves of 0 %, 20 %, 40 %, 60 %, 80 %, and 100 % ethanol solution in the frequency range of 1.4–2.8 GHz, as shown in Fig. 7(a). With increasing ethanol concentration, the resonant frequency exhibited a blue shift, from 1.56 GHz to 2.41 GHz, with the resonant frequency reaching 850 MHz. To verify the accuracy of the simulation, we processed the designed sensor and measured the equipment as shown in Fig. 7(b). In the experiment, an Agilent N3656B vector network analyzer is employed for measuring the S11 parameter. We poured configured ethanol solutions with 0 %, 20 %, 40 %, 60 %, 80 %, and 100 % concentrations into a closed container. The solution flowed into the cavity through the narrow edge gap of the cavity. The cavity is located directly below the sensor, with a volume of 24 mL as the sensor area for rapid detection and analysis of ethanol solutions with different concentrations. The test reflection spectra are shown in Fig. 7(c), where different ethanol solution concentrations can be well distinguished. The resonant frequencies were 1.56 GHz, 1.64 GHz, 1.82 GHz, 2.06 GHz, 2.2 GHz, and 2.44 GHz, respectively, with corresponding amplitudes of 13.90 dB, 26.92 dB, 17.17 dB, 17.53 dB, 22.11 dB, and 39.06 dB, as the concentration of ethanol solution increased. The trend of the experimental data was consistent with the simulation results, indicating that the proposed sensor is feasible for detecting 0 %-100 % ethanol solution. Due to the change of the medium below the metamaterial, the decrease of the dielectric constant and the change of the loss with the increase of the concentration of ethanol solution caused the obvious blue shift of the resonance frequency and the change of the amplitude. To observe the influence of ethanol concentration on the sensing effect, we plotted the relationship between the variation of resonance frequency and ethanol concentration as shown in Fig. 7(d). As ethanol concentration increased from 0 % to 60 %, the resonance frequency shift increased, whereas when it increased from 60 % to 80 %, the resonance frequency shift became relatively small, and then increased again when the concentration reached 100 %. The resonant frequency shift for the change of ethanol concentration from 0 % to 100 % reached 0.88 GHz, which is a larger common frequency shift compared to sensors in the same frequency band. Therefore, the designed sensor can detect ethanol solution more sensitively.

According to the values obtained from Fig. 7(c), the Q-factor, sensitivity and frequency detection resolution (FDR) can be extracted from [49] and represented by formulas 12,13 and 14, respectively. Where f_0 is the center frequency, and Δf is the bandwidth. Also, f_{01} and f_{02} are frequency for the first and second samples, and $\Delta\varepsilon_r$ is their permittivity difference. According to the results, f_{01} is 1.56 GHz, and f_{02} is 2.44 GHz, also $\Delta\varepsilon_r$ is 71, therefore seen that the Q-factor of the proposed sensor is 40, its sensitivity is 0.8 % and FDR is 0.012 GHz.

Table 3
Comparison of the proposed sensor with previous works.

Reference	Frequency (GHz)	Sensitivity (%)	Sample volume (mL)	Error (%)	Feeding method	Sensing application
[40]	2.38	0.02	0.236	2	Microstrip line	Ethanol
[43]	2.42	0.9	<1000	2.6	Microstrip line	Ethanol
[37]	7.85	0.3	< 1	2.6	Microstrip line	Ethanol and other liquids
[34]	3.18	0.57	< 2	2.2	Microstrip line	Ethanol
[50]	3	4	0.03	1.5	Microstrip line	Ethanol
[49]	6.21	0.64	0.064	2.1	Microstrip line	Glucose
[51]	2.8	2.2	21	5	Microstrip line	Vinegar
[52]	2.1	0.48	0.0044	2.85	Microstrip line	Equol
[53]	2.39	0.08	0.059	1.35	Microstrip line	Ethanol
This work	2.76	0.8	>24	0.88	Waveguide	Ethanol

$$\mathrm{Q-factor} = \frac{f_0}{\Delta f} \tag{12}$$

$$\mathrm{Sensitivity} = \left|\frac{(f_{01} - f_{02})}{f_{01}} \frac{1}{\Delta\varepsilon_r}\right| \times 100\% \tag{13}$$

$$\mathrm{FDR} = \frac{f_{01} - f_{02}}{\Delta\varepsilon_r} \tag{14}$$

For determining validity of the sensor, the measurement and simulation results are compared on each other, when their different is low, this shows the error value is small. The error is depicted with the difference between the sample simulation resonance frequency (f_{SS}) and sample measurement resonance frequency (f_{SM}) to free load resonance frequency (f_{FL}) that is illustrated in equation (15). The error of the each ethanol solution are depicted in Table 2, and it can be seen from the table that the average measurement error is only 0.88 %.

$$\mathrm{Error} = \frac{|f_{SM} - f_{SS}|}{f_{FL}}[\%] \tag{15}$$

To investigate the effect of changing the solution volume on the resonance frequency result, two different volumes of ethanol solution have been measured by the sensor. Fig. 7(e) shows the result of two different volumes of ethanol solution. It can be seen that changing the volume of ethanol solution has a negligible effect on the resonance frequency changes.

The results of calculation and measurement show that the designed sensor has a high sensitivity and is able to detect 0–100 % ethanol concentration samples with high sensitivity. Therefore, if this sensor is included in Fig. 7(b), it can be used in industry and measure the purity of aqueous solution, especially ethanol. Table 3 shows a comparison between the proposed sensor and previous works, and it can be seen that the designed sensor has greater sensitivity in most cases, while in a few cases with lower sensitivity, the error of the proposed sensor is much smaller. Moreover, the designed sensor not only has no certain limit on the volume of the solution, but also does not use additional pipelines as fluid channels. In addition, due to the constant volume of the cavity and metal shielding, compared to using microstrip line feeding method. The testing device can maintain stability, which is conducive to accurate detection in complex environments.

4.3. Comparison of the proposed device with conventional structure experiments

In order to better demonstrate the device we proposed for the rapid and sensitive detection of ethanol solutions, we conducted experimental comparisons with conventional devices used for ethanol solution detection. The conventional device involves placing the ethanol solution above the metamaterial structure and measuring primarily in free space. However, in our work, the measured object is placed below the metamaterial structure, with two gaps opened on both sides of the cavity. This arrangement enables repeated replacement of the ethanol solution without any impact on the metamaterial. Additionally, the ethanol solution is tested within the resonant cavity, which eliminates the influence of external environmental factors on the test. The comparison of the resonance frequency shift between the proposed ethanol solution detection method and the traditional free-space detection method is illustrated in Fig. 7(e). The results show that the resonance frequency shift is greater for our proposed method when the concentration of the ethanol solution changes from 0 % to 100 %, compared to the traditional detection method.

5. Conclusion

In our work, we developed a highly sensitive method for detecting ethanol solution that combines a waveguide resonant cavity with a metamaterial. By creating a gap on both sides of the narrow end of the resonant cavity, the liquid can flow into the cavity without the need for additional pipes as fluid channels, thus eliminating the potential influence of pipes on the detection sensitivity of ethanol solution. Furthermore, the constant volume and metal shielding of the cavity enable accurate detection in complex environments. To enhance the interaction between electromagnetic waves and the ethanol solution, a metamaterial based on the SRR structure is integrated with the cavity. A theoretical model of the multilayer medium is also constructed to analyze the propagation characteristics of electromagnetic waves and optimize performance. The multilayer medium equivalent model shows that it is feasible to achieve high-sensitivity detection of 0 %–100 % ethanol solution by combining the waveguide resonant cavity with metamaterial. Compared to traditional ethanol solution detection methods, the resonant frequency shift in our method is twice as high. While the waveguide resonant cavity detection method is more accurate than conventional methods, the overall size of the waveguide is large, which limits its size due to the wide bandwidth required to measure 0 %–100 % ethanol solution. Therefore, we plan to explore the use of microstrip lines for ethanol solution detection, which would make the overall device more compact.

CRediT authorship contribution statement

Yao Zhang: Conceptualization, Methodology, Validation, Formal analysis, Writing – original draft, Writing – review & editing. **Leijun Xu:** Conceptualization, Validation, Writing – review & editing. **Jianfeng Chen:** Conceptualization, Validation, Writing – review & editing. **Xue Bai:** Supervision, Writing – review & editing. **Xiao Zhou:** Conceptualization, Validation, Writing – review & editing.

Declaration of Competing Interest

The authors declare that they have no known competing financial interests or personal relationships that could have appeared to influence the work reported in this paper.

Data availability

The authors do not have permission to share data.

Acknowledgment

The authors gratefully acknowledge the financial support provided by the National Natural Science Foundation of China (Grant No.61874050), and the Graduate Research and Innovation Project of Jiangsu Province (Grant No. KYCX23_3659).

References

[1] S. Hosseini, S.J. Han, A. Arponwichanop, T. Yonezawa, S. Kheawhom, Ethanol as an electrolyte additive for alkaline zinc-air flow batteries, Sci. Rep. 8 (2018) 1–11, https://doi.org/10.1038/s41598-018-29630-0.
[2] N.K. Mahdy, M. El-Sayed, S.E. Al-Mofty, A. Mohamed, A.H. Karaly, M.E. El-Naggar, H. Nageh, W.A. Sarhan, H.M. El-Said Azzazy, Toward scaling up the production of metal oxide nanoparticles for application on washable antimicrobial cotton fabrics, ACS Omega 7 (2022) 38942–38956, https://doi.org/10.1021/acsomega.2c04692.
[3] Y. Cao, H. Mu, J. Guo, H. Liu, R. Zhang, W. Liu, M. Xian, H. Liu, Metabolic engineering of *Escherichia coli* for the utilization of ethanol, J. Biol. Res. (thessalon). 27 (2020) 1–10, https://doi.org/10.1186/s40709-020-0111-0.
[4] S.M. Hosseini, E. Taghiabadi, K. Abnous, A.T. Hariri, H. Pourbakhsh, H. Hosseinzadeh, Protective effect of thymoquinone, the active constituent of Nigella sativa fixed oil, against ethanol toxicity in rats, Iran J. Basic Med. Sci. 20 (2017) 927–939, https://doi.org/10.22038/IJBMS.2017.9116.
[5] M. Zhou, K. Cheng, H. Sun, G. Jia, Investigation of nonlinear output-input microwave power of DMSO-ethanol mixture by molecular dynamics simulation, Sci. Rep. 8 (2018) 1–10, https://doi.org/10.1038/s41598-018-21846-4.
[6] N. Martin-Gonzalez, L. Vieira Goncalves, G.N. Condezo, C. San Martin, M. Rubiano, I. Fallis, J.R. Rubino, M.K. Ijaz, J.Y. Maillard, P.J. De Pablo, Virucidal action mechanism of alcohol and divalent cations against human adenovirus, Front. Mol. Biosci. 7 (2020) 1–9, https://doi.org/10.3389/fmolb.2020.570914.

[7] A. Tejero Rioseras, D. Garcia Gomez, B.E. Ebert, L.M. Blank, A.J. Ibanez, P. M. Sinues, Comprehensive real-time analysis of the yeast volatilome, Sci. Rep. 7 (2017) 1–9, https://doi.org/10.1038/s41598-017-14554-y.

[8] T.Y. Yeh, M.F. Liu, R.D. Lin, S.J. Hwang, Alcohol selective optical sensor based on porous cholesteric liquid crystal polymer networks, Molecules 27 (2022) 1–13, https://doi.org/10.3390/molecules27030773.

[9] D. Mueller, W.A. Breeman, I. Klette, M. Gottschaldt, A. Odparlik, M. Baehre, I. Tworowska, M.K. Schultz, Radiolabeling of DOTA-like conjugated peptides with generator-produced ^{68}Ga and using NaCl-based cationic elution method, Nat. Protoc. 11 (2016) 1057–1066, https://doi.org/10.1038/nprot.2016.060.

[10] R. Tagaino, J. Washio, H. Otani, K. Sasaki, N. Takahashi, Bifacial biological effects of ethanol: acetaldehyde production by oral Streptococcus species and the antibacterial effects of ethanol against these bacteria, J. Oral Microbiol. 13 (2021) 1–8, https://doi.org/10.1080/20002297.2021.1937884.

[11] V. Galstyan, E. Comini, I. Kholmanov, A. Ponzoni, V. Sberveglieri, N. Poli, G. Faglia, G. Sberveglieri, A composite structure based on reduced graphene oxide and metal oxide nanomaterials for chemical sensors, Beilstein. J. Nanotechnol. 7 (2016) 1421–1427, https://doi.org/10.3762/bjnano.7.133.

[12] H. Zhang, S.H. Xiong, X.J. Jiang, L. Li, Y.Y. Zhang, F.J. Lyu, A painless and time-saving modified technique for simple renal cyst treatment with single-session ethanol sclerotherapy, Sci. Rep. 10 (2020) 1–8, https://doi.org/10.1038/s41598-020-61842-1.

[13] L.C. Melon, J.T. Nasman, A.S. John, K. Mbonu, J.L. Maguire, Interneuronal delta-GABA(A) receptors regulate binge drinking and are necessary for the behavioral effects of early withdrawal, Neuropsychopharmacology 44 (2019) 425–434, https://doi.org/10.1038/s41386-018-0164-z.

[14] B.A. Nasui, M. Popa, A.D. Buzoianu, A.L. Pop, V.N. Varlas, S.M. Armean, C. A. Popescu, Alcohol consumption and behavioral consequences in Romanian medical university students, Int. J. Environ. Res. Public Health 18 (2021) 1–14, https://doi.org/10.3390/ijerph18147531.

[15] Y. Zhang, M. Bi, Z. Chen, M. Dai, G. Zhou, Y. Hu, H. Yang, W. Guan, Hydrogen gas alleviates acute alcohol-induced liver injury by inhibiting JNK activation, Exp. Ther. Med. 21 (2021) 1–7, https://doi.org/10.3892/etm.2021.9884.

[16] H.G. Aleme, L.M. Costa, P.J. Barbeira, Determination of ethanol and specific gravity in gasoline by distillation curves and multivariate analysis, Talanta 78 (2009) 1422–1428, https://doi.org/10.1016/j.talanta.2009.02.042.

[17] X. Yi, J. Kong, Y. Song, J. Wang, L. Sun, Isobaric vapor-liquid equilibria and extractive distillation process design for separating ethanol and diethoxymethane, J. Chem. Eng. Data 66 (2021) 4326–4334, https://doi.org/10.1021/acs.jced.1c00443.

[18] M. Sriariyanun, P. Mutrakulcharoen, S. Tepaamorndech, K. Cheenkachorn, K. Rattanaporn, A rapid spectrophotometric method for quantitative determination of ethanol in fermentation products, Orient. J. Chem. 35 (2019) 744–750, https://doi.org/10.13005/ojc/350234.

[19] Y. Ciawi, W.S. Rita, S.A.P.M.S. Anggreni, Sugar concentration of Gracilaria sp. following hydrolysis using cellulase and sulphuric acid and several pretreatment methods, IOP Conf. Series: Earth Environ. Sci. 339 (2019) 1–9, https://doi.org/10.1088/1755-1315/339/1/012052.

[20] L. Hu, T. Li, Q. Luo, J. Zhang, Antioxidant stability of colloidal tea polyphenols in tea seed oil, J. Food Process. Preserv. 45 (2020) 1–8, https://doi.org/10.1111/jfpp.15130.

[21] M. Ming, X. Wang, L. Lian, H. Zhang, W. Gao, B. Zhu, D. Lou, Metabolic responses of Saccharomyces cerevisiae to ethanol stress using gas chromatography-mass spectrometry, Mol. Omics. 15 (2019) 216–221, https://doi.org/10.1039/c9mo00055k.

[22] C. Wunder, W. Pogoda, A. Paulke, S.W. Toennes, Assay of ethanol and congener alcohols in serum and beverages by headspace gas chromatography/mass spectrometry, MethodsX. 8 (2021) 1–7, https://doi.org/10.1016/j.mex.2021.101563.

[23] K.P. Zhou, X.F. Bai, W.H. Bi, Determination of ethanol content in ethanol-gasoline based on derivative absorption spectrometry and information fusion, Optoelectron. Lett. 14 (2018) 442–446, https://doi.org/10.1007/s11801-018-8081-2.

[24] H. Sheng, S. Ma, T. Han, P. Yun, T. Yang, J. Ren, A highly sensitivity and anti-humidity gas sensor for ethanol detection with $NdFeO_3$ nano-coral granules, Vacuum 195 (2022) 1–9, https://doi.org/10.1016/j.vacuum.2021.110642.

[25] H.A. Zain, M. Batumalay, H.R.A. Rahim, M. Yasin, S.W. Harun, Single-walled carbon nanotubes coated D-shaped fiber for aqueous ethanol detection, Optoelectron. Lett. 18 (2022) 430–433, https://doi.org/10.1007/s11801-022-1166-y.

[26] W. Zhan, Z. Chen, J. Hu, X. Chen, Vertical CuO nanowires array electrodes: Visible light sensitive photoelectrochemical biosensor of ethanol detection, Mater. Sci. Semicond. Process. 85 (2018) 90–97, https://doi.org/10.1016/j.mssp.2018.06.002.

[27] Y. Febriani, E.A. Ihsan, Determination of ethanol in a distillate sample of arenga pinnata by UV-visible spectrophotometry, J. Phys. Conf. Ser. 1539 (2020) 1–7, https://doi.org/10.1088/1742-6596/1539/1/012002.

[28] Y. Hayashi, T. Komatsu, K. Iwashita, E. Fukusaki, 1H-NMR metabolomics-based classification of Japanese sake and comparative metabolome analysis by gas chromatography-mass spectrometry, J. Biosci. Bioeng. 131 (2021) 557–564, https://doi.org/10.1016/j.jbiosc.2020.12.008.

[29] G. Li, G. Wang, T. Yang, Y. Zhang, J. Shen, B. Zhang, Graphene-based terahertz bias-driven negative-conductivity metasurface, Nanoscale Adv. 4 (2022) 3342–3352, https://doi.org/10.1039/d2na00288d.

[30] Q. Xie, G.X. Dong, B.X. Wang, W.Q. Huang, High-Q fano resonance in terahertz frequency based on an asymmetric metamaterial resonator, Nanoscale Res. Lett. 13 (2018) 1–7, https://doi.org/10.1186/s11671-018-2677-0.

[31] G. Deng, K. Lv, H. Sun, J. Yang, Z. Yin, Y. Li, B. Chi, X. Li, An ultrathin triple-band metamaterial absorber with wide-incident-angle stability for conformal applications at X and Ku frequency band, Nanoscale Res. Lett. 15 (2020) 1–10, https://doi.org/10.1186/s11671-020-03448-0.

[32] M. Abdolrazzaghi, M. Daneshmand, A.K. Iyer, Strongly enhanced sensitivity in planar microwave sensors based on metamaterial coupling, IEEE Trans. Microw. Theory Tech. 66 (2018) 1843–1855, https://doi.org/10.1109/tmtt.2018.2791942.

[33] A. Ebrahimi, J. Scott, K. Ghorbani, Ultrahigh-sensitivity microwave sensor for microfluidic complex permittivity measurement, IEEE Trans. Microw. Theory Tech. 67 (2019) 4269–4277, https://doi.org/10.1109/tmtt.2019.2932737.

[34] Q. Jiang, Y. Yu, Y. Zhao, Y. Zhang, L. Liu, Z. Li, Ultra-compact effective localized surface plasmonic sensor for permittivity measurement of aqueous ethanol solution with high sensitivity, IEEE Trans. Instrum. Meas. 70 (2021) 1–9, https://doi.org/10.1109/tim.2021.3092783.

[35] S. Kiani, P. Rezaei, Microwave substrate integrated waveguide resonator sensor for non-invasive monitoring of blood glucose concentration: Low cost and painless tool for diabetics, Measurement 219 (2023) 1–8, https://doi.org/10.1016/j.measurement.2023.113232.

[36] S. Kiani, P. Rezaei, M. Fakhr, Dual-frequency microwave resonant sensor to detect noninvasive glucose-level changes through the fingertip, IEEE Trans. Instrum. Meas. 70 (2021) 1–8, https://doi.org/10.1109/tim.2021.3052011.

[37] S. Kiani, P. Rezaei, M. Navaei, Dual-sensing and dual-frequency microwave SRR sensor for liquid samples permittivity detection, Measurement 160 (2020) 1–7, https://doi.org/10.1016/j.measurement.2020.107805.

[38] J. Liang, P. Lv, M. Bai, H. Duan, Tunable microwave absorbing metamaterial composed of micro-channels filled with replaceable water solution, Mater. Lett. 307 (2022) 1–4, https://doi.org/10.1016/j.matlet.2021.131016.

[39] S. Mohammadi, K.K. Adhikari, M.C. Jain, M.H. Zarifi, High-resolution, sensitivity-enhanced active resonator sensor using substrate-embedded channel for characterizing low-concentration liquid mixtures, IEEE Trans. Microw. Theory Tech. 70 (2022) 576–586, https://doi.org/10.1109/tmtt.2021.3109599.

[40] E.L. Chuma, Y. Iano, G. Fontgalland, L.L. Bravo Roger, Microwave sensor for liquid dielectric characterization based on metamaterial complementary split ring resonator, IEEE Sens. J. 18 (2018) 9978–9983, https://doi.org/10.1109/jsen.2018.2872859.

[41] Y. Khanna, Y.K. Awasthi, Dual-band microwave sensor for investigation of liquid impurity concentration using a metamaterial complementary split-ring resonator, J. Electron. Mater. 49 (2019) 385–394, https://doi.org/10.1007/s11664-019-07761-y.

[42] Y.I. Abdulkarim, M. Bakir, I. Yasar, H. Ulutas, M. Karaaslan, F. Ozkan Alkurt, C. Sabah, J. Dong, Highly sensitive metamaterial-based microwave sensor for the application of milk and dairy products, Appl. Opt. 61 (2022) 1972–1981, https://doi.org/10.1364/AO.451900.

[43] S.Y. Jang, J.R. Yang, Double split-ring resonator for dielectric constant measurement of solids and liquids, J. Electromagn. Eng. Sci. 22 (2022) 122–128, https://doi.org/10.26866/jees.2022.2.r.68.

[44] X. Chen, Y. Gu, J. Liang, M. Bai, S. Wang, M. Li, Z. Zhang, Enhanced microwave shielding effectiveness and suppressed reflection of chopped carbon fiber felt by electrostatic flocking of carbon fiber, Compos. A Appl. Sci. Manuf. 139 (2020) 1–11, https://doi.org/10.1016/j.compositesa.2020.106099.

[45] D. Fan, A new approach to diffraction analysis of conductor grids. II. Perpendicular-polarized incident plane waves, IEEE Transact. Antennas & Propag. 37 (1989) 89–93, https://doi.org/10.1109/8.192169.

[46] H.R. Heidari, P. Rezaei, S. Kiani, M. Taherinezhad, A monopulse array antenna based on SIW with circular polarization for using in tracking systems, AEU-Int. J. Electron. C. 162 (2023) 1–9, https://doi.org/10.1016/j.aeue.2023.154563.

[47] J.Z. Bao, M.L. Swicord, C.C. Davis, Microwave dielectric characterization of binary mixtures of water, methanol, and ethanol, J. Chem. Phys. 104 (1996) 4441–4450, https://doi.org/10.1063/1.471197.

[48] Q. Chen, Z. Long, N. Shinohara, C. Liu, A substrate integrated waveguide resonator sensor for dual-band complex permittivity measurement, Processes 10 (2022) 1–10, https://doi.org/10.3390/pr10040708.

[49] S. Kiani, P. Rezaei, M. Fakhr, Real-time measurement of liquid permittivity through label-free meandered microwave sensor, IETE J. Res. (2023) 1–11, https://doi.org/10.1080/03772063.2023.2231875.

[50] M. Navaei, P. Rezaei, S. Kiani, Measurement of low-loss aqueous solutions permittivity with high detection accuracy by a contact and free-label resonance microwave sensor, Int. J. Commun Syst 36 (2022) 1–12, https://doi.org/10.1002/dac.5417.

[51] M. Navaei, P. Rezaei, S. Kiani, A symmetric bar chart-shape microwave sensor with high Q-factor for permittivity determination of fluidics, Int. J. Microw. Wirel. Technol. 15 (2023) 1334–1342, https://doi.org/10.1017/s1759078723000053.

[52] P. Loutchanwoot, S. Harnsoongnoen, Microwave microfluidic sensor for detection of high equol concentrations in aqueous solution, IEEE Trans. Biomed. Circuits Syst. 16 (2022) 244–251, https://doi.org/10.1109/tbcas.2022.3153459.

[53] S. Mosbah, C. Zebiri, D. Sayad, I. Elfergani, M.L. Bouknia, S. Mekki, R. Zegadi, M. Palandoken, J. Rodriguez, R.A. Abd-Alhameed, Compact and highly sensitive bended microwave liquid sensor based on a metamaterial complementary split-ring resonator, Appl. Sci. 12 (2022) 1–16, https://doi.org/10.3390/app12042144.